Yb^{3+}-sensitized visible Ni^{2+} photon upconversion in codoped $CsCdBr_3$ and $CsMgBr_3$

Sara García-Revilla,[1] Pascal Gerner,[2] Hans U. Güdel,[2] and Rafael Valiente[1]
[1]*Departamento de Física Aplicada, Universidad de Cantabria, Avda. de los Castros s/n, Santander 39005, Spain*
[2]*Departement für Chemie und Biochemie, Universität Bern, Freiestrasse 3, CH-3000 Bern 9, Switzerland*
(Received 16 May 2005; published 14 September 2005)

Near-infrared excitation of Yb^{3+} $^2F_{7/2} \rightarrow {}^2F_{5/2}$ at 10 600 cm^{-1} in the linear chain $CsMBr_3:Ni^{2+},Yb^{3+}$ (M =Cd,Mg) structure leads to green luminescence from Yb^{3+} pairs and red Ni^{2+} upconversion luminescence at cryogenic temperatures. The broad red upconversion luminescence is assigned to the $^1T_{2g} \rightarrow {}^3A_{2g}$ transition of Ni^{2+}. The upconversion excitation spectrum indicates that the active mechanism in these systems involves both Yb^{3+} and Ni^{2+} ions. Lifetime and power dependence data allow one to identify a ground-state-absorption (GSA) energy-transfer upconversion (ETU) as the underlying upconversion mechanism for the Yb^{3+}-Ni^{2+} system in doubly doped $CsCdBr_3$ and $CsMgBr_3$. A less efficient single-ion GSA excited-state-absorption (ESA) process within Ni^{2+} is also observed in the title compounds. However, whereas the GSA/ESA process requires an excitation energy above 11 200 cm^{-1}, it is possible to sensitize the Ni^{2+} upconversion via Yb^{3+} excitation at energies around 10 200 cm^{-1} and around 10 600 cm^{-1} in $CsCdBr_3$ and $CsMgBr_3$. It is shown that only those Ni^{2+} ions neighboring to Yb^{3+} ions are relevant for the upconversion induced by Yb^{3+} excitation.

DOI: 10.1103/PhysRevB.72.125111 PACS number(s): 78.55.−m, 42.65.Ky

I. INTRODUCTION

Photon upconversion (UC) provides an efficient way to convert long wavelength input radiation into shorter wavelength output light, which does not require coherent input radiation.[1] A variety of devices based on UC such as several lasers,[2] imaging material devices,[3] phosphors,[4] and IR quantum-counting devices[5] have been developed. A defining characteristic for all UC systems is the existence of a metastable intermediate state that serves as a storage reservoir for the pump energy and at least one more higher lying emitting state. This is a common phenomenon in systems involving f-f transitions in trivalent rare-earth (R) ions due to their well-shielded $4f$ electrons.[6,7] However, light emission from multiple excited states is unusual among transition-metal (TM) ions due to the stronger electron-phonon coupling of the d electrons. Thus only few examples of UC in TM ions have been reported in the literature.[8–12]

Among the different mechanisms proposed since the first report of UC processes in 1966,[13] the ground-state absorption (GSA) and excited state absorption (ESA), and energy transfer upconversion (ETU) and cooperative sensitization are the most relevant for the discussion in the present paper. To distinguish these UC mechanisms a combination of excitation and temporal evolution measurements is usually used.[6]

The combination of TM and R ions within the same compound, has led to very new and unexpected results in the search for novel UC materials and processes. These systems take advantage of the invariance to the chemical environment of lanthanide ions combined with the chemical tunability of the energy levels in TM ions. First examples of visible UC in mixed TM-R systems have been reported for Mn^{2+}-Yb^{3+},[14–24] Cr^{3+}-Yb^{3+},[25–27] Re^{4+}-Yb^{3+},[28] and V^{3+}-Er^{3+}.[29] All Yb^{3+} containing systems involve excitation around 1 μm resonant with the absorption peaks of Yb^{3+} which sensitizes the visible UC emission from the TM ion. In Mn^{2+}-Yb^{3+} UC systems a UC mechanism based on Mn^{2+}-Yb^{3+} exchange interaction was described. On the other hand in $Y_3Ga_5O_{12}$ codoped with Cr^{3+} and Yb^{3+} a cooperative energy transfer from two Yb^{3+} ions to a Cr^{3+} ion has been identified. An energy transfer step from Yb^{3+} to Re^{4+} followed by an ETU process on Re^{4+} is responsible for the UC phenomenon observed in $Cs_2NaYbBr_6:Re^{4+}$.

Ni^{2+} has two metastable excited states in various low phonon host lattices. It thus is one of the TM that represents an exception to Kasha's rule,[30] which states that luminescence is to be expected, if at all, only from the lowest excited state. In 1963, Ni^{2+}-doped MgF_2 was reported as the first example of a laser with broadband tuning capability at low temperatures.[31] Later, laser operation was also achieved in $MgO:Ni^{2+}$ (Ref. 32) and in $KMgF_3:Ni^{2+}$ (Ref. 33) at liquid N_2 temperature. Since then, numerous reports devoted to the investigation of the optical spectroscopic properties of Ni^{2+} as a dopant ion in different host lattices appeared.[34–40] In the past few years Ni^{2+} UC has been intensively studied in different singly doped fluoride,[41] chloride,[15,17,42,43] and bromide[44,45] host lattices. This UC process (ascribed to a GSA-ESA mechanism) involves two spin forbidden transitions, which limits its efficiency. It was shown that pressure can be used to tune the UC properties, in particular, to increase the efficiency of the underlying process in $CsCdCl_3:Ni^{2+}$.[43,46]

The present study reports on the UC properties of the new codopant combination Ni^{2+}-Yb^{3+}. In a very recent paper, we reported preliminary results of UC in $CsCdBr_3:Ni^{2+},Yb^{3+}$.[47] A detailed analysis of the spectroscopic data of Ni^{2+} and Yb^{3+} codoped $CsMgBr_3$ and $CsCdBr_3$ leads to the understanding of the underlying UC process.

II. EXPERIMENT

A. Crystal growth and manipulation

Single crystals of doubly doped $CsMBr_3:Ni^{2+},Yb^{3+}$ (M =Mg, Cd) were grown by the Bridgman technique using sto-

ichiometric amounts of CsBr, $MgBr_2$, and $CdBr_2$, and nominal concentrations of 1 and 5 % of $YbBr_3$ and $NiBr_2$, respectively. All dopant concentrations are given in mole percent. Crystals of centimetre size and good optical quality were obtained. As expected, the crystal quality decreases for higher Yb^{3+} concentrations. The crystal structure was checked by x-ray powder diffraction. Due to the hygroscopic nature of the starting materials, all the handling was carried out under a dry inert atmosphere in a glovebox. Furthermore, crystals were mounted in a closed copper cell or closed quartz ampoules filled with He gas for absorption and emission measurements, respectively. Actual dopant concentrations were determined to be 3.8% Ni^{2+} and 0.3% Yb^{3+} in the case of $CsCdBr_3$ and 4.9% Ni^{2+} and 0.6% Yb^{3+} for the $CsMgBr_3$.

B. Spectroscopic measurements

Absorption spectra were measured on a Cary 5e (Varian) spectrometer. Samples were cooled with a closed cycle cryostat (Air Products Displex). Continuous-wave Yb^{3+} and Ni^{2+} luminescence and excitation spectra were carried out with a tunable Ti: sapphire laser (Spectra Physics 3900S) pumped by a $Nd:YVO_4$ laser (Spectra Physics Millenia XS-FRU, second harmonic). The emission was dispersed by a 0.85 m double monochromator (Spex 1402) using 1200 grooves/mm gratings blazed at 750 nm and detected by a cooled photomultiplier (Hamamatsu 3310-01) and a photon counting system (Stanford Research SR400). Ni^{2+} luminescence was also excited by the 488 nm line of an Ar^+-ion laser (Spectra Physics 2045-15) and detected as described above. The Ni^{2+} NIR $^3T_{2g} \rightarrow {}^3A_{2g}$ luminescence transition was analyzed with a 0.75 m single monochromator (Spex 1702) equipped with 600 grooves/mm grating blazed at 1250 nm and detected using an InAs detector (Hamamatsu P7163) connected to a lock-in amplifier (Stanford Research SR830). The laser beam was focused on the sample with a 53 mm focal length lens. The typical excitation density was 4.7 kW/cm^2. Power-dependent measurements were performed using calibrated neutral density filters (Balzers) to attenuate the laser excitation power. The power was measured with a power meter (Coherent Labmaster-E). All the luminescence spectra were corrected for the sensitivity of the monochromator and the detection system and for the refractive index of air (vacuum correction). However, the emission intensities are not corrected for the temperature dependence of the absorption cross sections at the excitation energies. For excitation spectra, the Ti: sapphire laser was scanned using a step-motor-driven birefringent filter and the wavelength was monitored with a wavemeter (Burleigh WA2100). The wavelength dependence of the laser power was measured simultaneously with the excitation scans in order to correct the spectra. For lifetime experiments, rectangular Ti: sapphire laser pulses were generated by using an acousto-optic modulator (Coherent 305) connected to a function generator (Stanford Research DS 430). Luminescence decay curves were recorded on a multichannel scaler (Stanford Research SR430). For all the luminescence measurements, crystal cooling was achieved using the helium flow tube technique.

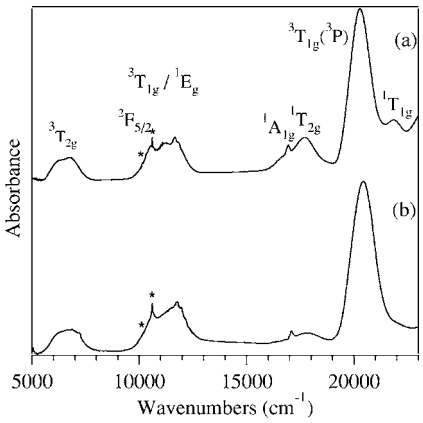

FIG. 1. 12 K unpolarized survey absorption spectra of $CsCdBr_3:3.8\%\ Ni^{2+}, 0.3\%\ Yb^{3+}$ (a) and $CsMgBr_3:4.9\%\ Ni^{2+}, 0.6\%\ Yb^{3+}$ (b). Yb^{3+} transitions are marked with asterisks. The excited states of Ni^{2+} and Yb^{3+} are labeled.

III. RESULTS

Figure 1 shows unpolarized survey absorption spectra at 12 K of Ni^{2+} and Yb^{3+} codoped crystals of $CsCdBr_3$ (a) and $CsMgBr_3$ (b). Although the site symmetry of the divalent cation is D_{3d}, for convenience, we use O_h notation for states labeling.[48] According to the d^8 Tanabe-Sugano energy level diagram[49] [Fig. 2(a)], the assignment of the seven Ni^{2+} absorption bands is given in Fig. 1. The sharp absorption features marked with asterisks, observed around 10 200 and 10 600 cm^{-1}, are due to the Yb^{3+} $^2F_{7/2} \rightarrow {}^2F_{5/2}$ transitions.

Figure 3 shows 12 K survey luminescence spectra of $CsCdBr_3:Ni^{2+}, Yb^{3+}$ after excitation of the dominant $^2F_{5/2}$ absorption feature of Yb^{3+} at 10 604 cm^{-1} (a) and after direct Ni^{2+} $^3T_{1g}(^3P)$ excitation at 20 491 cm^{-1} (b). In Fig. 4 the corresponding luminescence spectra for the $CsMgBr_3:Ni^{2+}, Yb^{3+}$ after excitation at 10 609 cm^{-1} (a) and at 20 491 cm^{-1} (b) are presented.

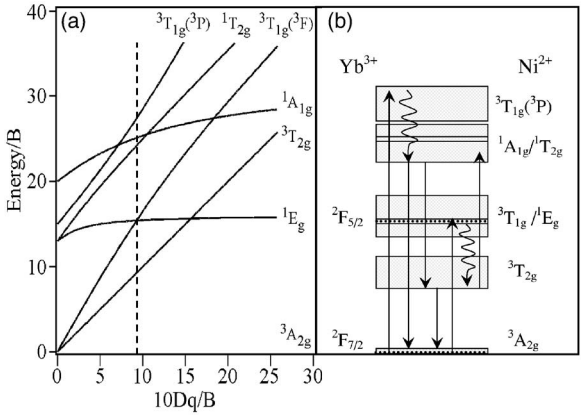

FIG. 2. (a) Tanabe-Sugano diagram for octahedrally coordinated Ni^{2+}. The dashed line corresponds to the crystal field in $Ni^{2+}:CsCdBr_3$ and $CsMgBr_3$. (b) Schematic representation of the energy-level diagram for both compounds. Horizontal dotted lines correspond to the Yb^{3+} $^2F_{7/2}$ and $^2F_{5/2}$ states. Solid arrows represent radiative processes, curly arrows multiphonon processes. Symmetry labels are given in the idealized O_h point group.

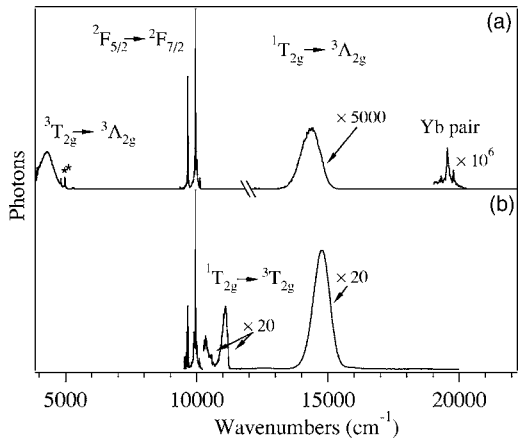

FIG. 3. 12 K unpolarized survey luminescence spectra in $CsCdBr_3$:3.8% Ni^{2+},0.3% Yb^{3+} after Yb^{3+} excitation at 10 604 cm^{-1} (a) and after direct Ni^{2+} $^3T_{1g}(^3P)$ excitation at 20 491 cm^{-1} (b). All the luminescence bands are assigned. Note the different scaling factors. The sharp features marked with asterisks correspond to the second order of the sharp lines around 10 000 cm^{-1}.

In Figs. 3(a) and 4(a) four different luminescence bands are identified in the luminescence spectra after Yb^{3+} excitation: (i) the broad band centered below 5000 cm^{-1} corresponds to the Ni^{2+} $^3T_{2g} \rightarrow {}^3A_{2g}$ transition, (ii) the sharp lines between 9350 and 10 200 cm^{-1} correspond to $^2F_{5/2}$ to $^2F_{7/2}$ transitions of Yb^{3+}, (iii) the weak broad band around 15 000 cm^{-1} is due to the red Ni^{2+} $^1T_{2g} \rightarrow {}^3A_{2g}$ UC luminescence and finally, (iv) around 20 000 cm^{-1} the very weak blue-greenish cooperative Yb^{3+} pair luminescence is observed.[50] Figure 2(b) schematically illustrates all these transitions.

The red Ni^{2+} $^1T_{2g}$ UC luminescence in Fig. 3(a) appears roughly 450 cm^{-1} lower in energy than the corresponding Ni^{2+} luminescence after direct Ni^{2+} excitation at 20 491 cm^{-1} in the $CsCdBr_3$ [Fig. 3(b)]. Analogously, Figs. 4(a) and 4(b)

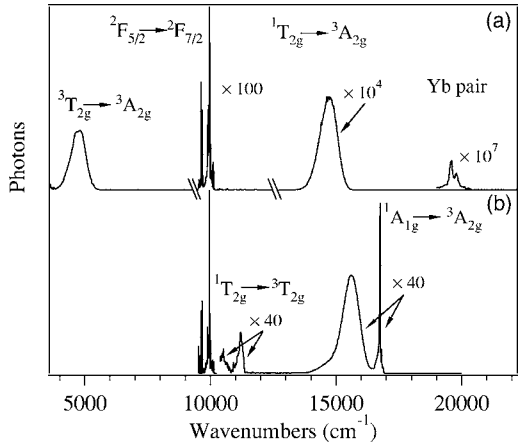

FIG. 4. 12 K unpolarized survey luminescence spectra in $CsMgBr_3$:4.9% Ni^{2+},0.6% Yb^{3+} after Yb^{3+} excitation at 10 609 cm^{-1} (a) and after direct Ni^{2+} $^3T_{1g}(^3P)$ excitation at 20 491 cm^{-1} (b). All the luminescence bands are assigned. Note the different scaling factors.

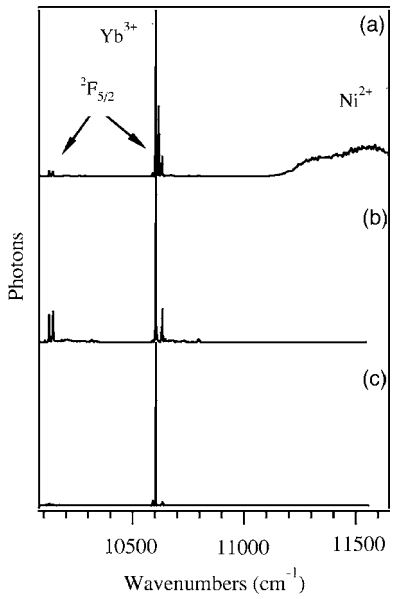

FIG. 5. 12 K excitation spectra of $CsCdBr_3$:3.8% Ni^{2+},0.3% Yb^{3+} monitoring (a) the Ni^{2+} UC $^1T_{2g}$ luminescence at 14 514 cm^{-1}, (b) the NIR Yb^{3+} luminescence at 9960 cm^{-1}, and (c) the Yb^{3+}-pair luminescence at 19 570 cm^{-1}.

show the corresponding redshift of 970 cm^{-1} in $CsMgBr_3$:Ni^{2+},Yb^{3+}. After direct Ni^{2+} excitation at 20 491 cm^{-1} in this compound, dual emission corresponding to $^1T_{2g} \rightarrow {}^3A_{2g}$ centered around 15 500 cm^{-1} and a sharp peak at 16 760 cm^{-1} assigned to the $^1A_{1g} \rightarrow {}^3A_{2g}$ transition is observed. After Yb^{3+} excitation no Ni^{2+} $^1A_{1g} \rightarrow {}^3A_{2g}$ luminescence is observed.

Although in both compounds the $^1T_{2g} \rightarrow {}^3T_{2g}$ interexcited state luminescence (around 11 000 cm^{-1}) is observed after green excitation at 20 491 cm^{-1} [Figs. 3(b) and 4(b)], it is not present in the respective UC luminescence spectra [Figs. 3(a) and 4(a)]. It is remarkable that NIR Yb^{3+} luminescence is observed after direct Ni^{2+} excitation into the $^3T_{1g}(^3P)$ in both compounds.

In Figs. 5(a), 5(b), and 5(c), the 12 K excitation spectra of $CsCdBr_3$:Ni^{2+},Yb^{3+} in the NIR around 10 000 cm^{-1} monitoring the red Ni^{2+} luminescence, the NIR Yb^{3+} luminescence, and the green Yb^{3+}-pair luminescence, respectively, are plotted. The corresponding excitation spectra for $CsMgBr_3$ are shown in Figs. 6(a), 6(b), and 6(c). The sharp lines present in these spectra are associated with the *f-f* absorption transitions of Yb^{3+}. Whereas the energies of the peaks are the same in the three spectra for each compound, the relative intensities are significantly different. Comparing Fig. 5(b) with Fig. 5(a), and Fig. 6(b) with Fig. 6(a), an additional sharp line feature is seen in the Ni^{2+} UC spectrum at 10 617 cm^{-1} [Fig. 5(a)] and 10 609 cm^{-1} [Fig. 6(a)] for $CsCdBr_3$ and $CsMgBr_3$, respectively. The broad UC excitation band above 11 200 cm^{-1} is due to a Ni^{2+} single ion UC process.

Figure 7 shows the normalized integrated Ni^{2+} $^1T_{2g} \rightarrow {}^3A_{2g}$ luminescence intensity as a function of temperature for direct Ni^{2+} excitation at 20 491 cm^{-1} (squares) and upconversion excitation at 10 604 cm^{-1} (crosses) in

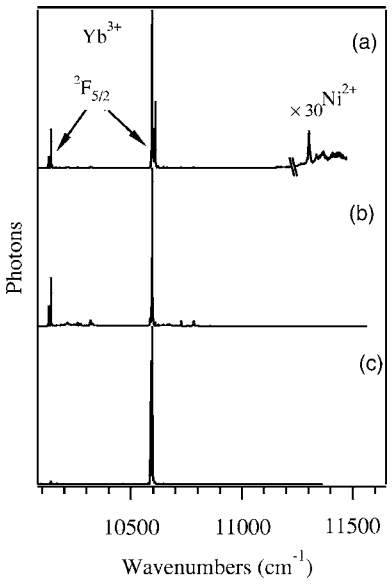

FIG. 6. 12 K excitation spectra of $CsMgBr_3$:4.9% Ni^{2+},0.6% Yb^{3+} monitoring (a) the Ni^{2+} UC $^1T_{2g}$ luminescence at 14 793 cm^{-1}, (b) the NIR Yb^{3+} luminescence at 9970 cm^{-1}, and (c) the Yb^{3+}-pair luminescence at 19 607 cm^{-1}.

$CsCdBr_3:Ni^{2+},Yb^{3+}$. Above 100 K the Ni^{2+} luminescence is quenched. Both curves present a similar temperature behavior, already observed for the singly doped $CsCdBr_3$:0.1% Ni^{2+},[44] although for excitation at 10 604 cm^{-1} the drop in Ni^{2+} UC luminescence intensity sets in at slightly lower temperatures. The temperature dependence of the $^1T_{2g}\rightarrow{}^3A_{2g}$ UC lifetime is similar (data not shown). The different behavior observed for the two modes of excitation is attributed to an energy transfer from Ni^{2+} to Yb^{3+}, which will be discussed in Sec. IV C.

Figure 8 shows the power dependence of the Yb^{3+} NIR (a), Ni^{2+} UC (b), and green cooperative Yb^{3+}-pair (c) luminescence intensity for 10 604 cm^{-1} excitation on a log-log scale for the $CsCdBr_3:Ni^{2+},Yb^{3+}$ at 12 K. Straight lines represent linear fits to the logarithmic data. The slope of the power dependence of the Yb^{3+} $^2F_{5/2}$ luminescence is 1.1 over the whole power range. Within experimental accuracy, for the two types of visible UC emission this system shows slope of 2 up to 3 kW/cm^2 excitation density. For higher excitation densities the slope of the Ni^{2+} UC is reduced to 1.3±0.1, whereas the slope of the cooperative Yb^{3+} pair luminescence remains 2.

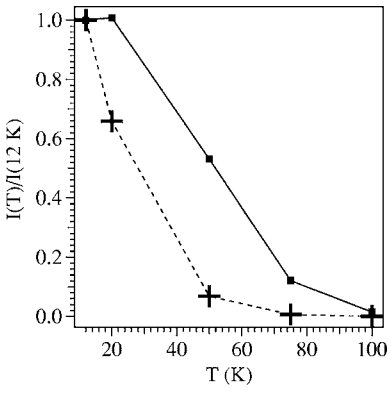

FIG. 7. Temperature dependence of the normalized integrated Ni^{2+} $^1T_{2g}\rightarrow{}^3A_{2g}$ luminescence intensities in $CsCdBr_3$:3.8% Ni^{2+},0.3% Yb^{3+} after Yb^{3+} excitation at 10 604 cm^{-1} (crosses) and after direct Ni^{2+} excitation at 20 491 cm^{-1} (squares). They are not corrected for the temperature dependence of the absorption cross section at the excitation energies.

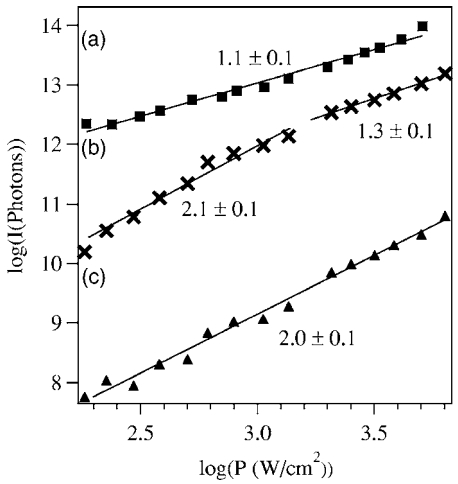

FIG. 8. 12 K excitation power dependence of the (a) NIR Yb^{3+} luminescence (b) Ni^{2+} $^1T_{2g}$ UC luminescence and (c) Yb^{3+}-pair luminescence, after Yb^{3+} excitation at 10 604 cm^{-1} for the $CsCdBr_3$:3.8% Ni^{2+},0.3% Yb^{3+} in a double logarithmic representation. The slopes of the corresponding linear fits are given.

Figure 9 compares the 12 K time dependence of the $^1T_{2g}\rightarrow{}^3A_{2g}$ emission intensity of $CsCdBr_3:Ni^{2+},Yb^{3+}$ after 15 ms square-wave excitation pulses at 10 604 cm^{-1} (a) and at 20 491 cm^{-1} (b). The dynamics of the Ni^{2+} UC, the Yb^{3+} $^2F_{5/2}\rightarrow{}^2F_{7/2}$ and the Yb^{3+}-pair luminescence show a double exponential behavior after NIR excitation. The slow and dominant contribution of all these decays, as well as the temporal evolution of Yb^{3+} after Ni^{2+} direct excitation are collected in Table I. The corresponding decay times measured in the $CsMgBr_3:Ni^{2+},Yb^{3+}$ are presented in Table II.

IV. DISCUSSION

A. Crystal structure and dopant distribution

$CsCdBr_3$ and $CsMgBr_3$ both crystallize in the hexagonal space group $P6_3/mmc$ and consist of linear chains of face-sharing $[MBr_6]^{4-}$ octahedra with the chains arranged along the crystallographic *c* axis, and the Cs^+ ions occupying high-symmetry sites between the chains.[48] Ni^{2+} dopant ions substitute the divalent cation site with D_{3d} symmetry. Yb^{3+} is incorporated into the M^{2+} lattice position forming charge-compensated ion-pair centers. EPR studies on $CsCdBr_3:Yb^{3+}$ (Refs. 51–53) and on Gd^{3+}-doped $CsCdBr_3$ and $CsMgBr_3$ (Ref. 54) show that the main impurity sites for the trivalent *R* ions in this structure are the so-called McPherson pairs,[54–56] i.e., symmetric in-chain Yb^{3+}-(M^{2+} vacancy)-Yb^{3+} ion pairs. Due to the different ionic radii of Cd^{2+} and Mg^{2+} as compared to the Ni^{2+} and Yb^{3+} radii, the octahedral

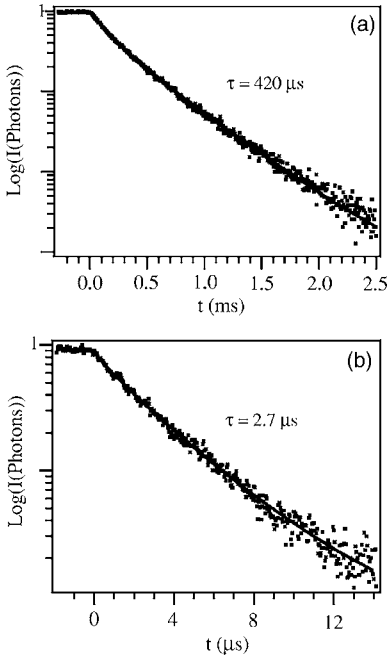

FIG. 9. 12 K temporal evolution in a semi logarithmic representation of the Ni^{2+} $^1T_{2g} \rightarrow {}^3A_{2g}$ luminescence in $CsCdBr_3:3.8\%$ Ni^{2+}, 0.3% Yb^{3+} after square pulse excitation at 10 604 cm^{-1} (a) and 20 491 cm^{-1} (b). The full lines correspond to a double exponential fit to the data. Note the different scale for the x axis.

coordination environment of the dopant ions is expected to be distorted.

Based on the dopant concentrations and assuming a statistical impurity center distribution, the percentage of Yb^{3+} with a Ni^{2+} next neighbor and vice versa can be estimated using a binomial distribution. As will be discussed, this is important for the understanding of the Ni^{2+} UC efficiency. From this calculation, it turns out that only 8% of the Yb^{3+} ions in the $CsCdBr_3$ compound have a Ni^{2+} ion as nearest neighbor. Conversely, just 0.3% of the total Ni^{2+} ions have an Yb^{3+} ion as nearest neighbor. Analogously, we estimate that in the $CsMgBr_3$, 10% of the Yb^{3+} ions have a Ni^{2+} ion nearest neighbor and 0.6% of the Ni^{2+} ions are adjacent to an Yb^{3+}. Therefore, we have to bear in mind that most of the Ni^{2+} ions are "isolated" (i.e., Ni^{2+} without a nearest Yb^{3+} neighbor) and are thus not involved in the most likely UC process.

TABLE I. 12 K decay times of the various metastable excited states in $CsCdBr_3:3.8\%Ni^{2+},0.3\%Yb^{3+}$ single crystal for different excitation energies (E_{exc}). E_{mon} corresponds to the detection energy.

	$E_{mon}(cm^{-1})$	$E_{exc}(cm^{-1})$	$\tau(\mu s)$
Yb^{3+}	9960	10 604	600±10
	9960	20 491	500±10
Yb^{3+} pairs	19570	10 604	285±5
Ni^{2+}	14514 ($^1T_{2g}$)	10 604	420±10
	14859 ($^1T_{2g}$)	20 491	2.7±0.1
	4325 ($^3T_{2g}$)	10 604	8100±100

TABLE II. 12 K decay times of the various metastable excited states in $CsMgBr_3:4.9\%Ni^{2+},0.6\%Yb^{3+}$ single crystal for different excitation energies (E_{exc}). E_{mon} corresponds to the detection energy.

	$E_{mon}(cm^{-1})$	$E_{exc}(cm^{-1})$	$\tau(\mu s)$
Yb^{3+}	9970	10 596	300±5
	9970	20 491	330±5
Yb^{3+} pairs	19 570	10 596	170±4
Ni^{2+}	14 706($^1T_{2g}$)	10 596	330±5
	15 674 ($^1T_{2g}$)	20 491	6.8±0.1

B. Yb^{3+} $^2F_{7/2} \leftrightarrow {}^2F_{5/2}$ transitions and dynamics

The excited state of Yb^{3+}, $^2F_{5/2}$, is split by the crystal field into three Kramers doublets. Therefore three electronic origins are expected in the Yb^{3+} excitation spectra and these are assigned to the sharp line features at 10 125, 10 141, and 10 604 cm^{-1} for the Cd^{2+} lattice and 10 131, 10 139, and 10 596 cm^{-1} for the Mg^{2+} lattice, respectively [see Figs. 5(b) and 6(b)]. These features are assigned to the electronic origins of the dominant Yb^{3+}-vacancy-Yb^{3+} defect center.

At 12 K both $CsCdBr_3:Ni^{2+},Yb^{3+}$ and $CsMgBr_3:Ni^{2+},Yb^{3+}$, exhibit an extremely weak green luminescence band after 10 604 cm^{-1} and 10 596 cm^{-1} excitation, respectively [see Figs. 3(a) and 4(a)]. This is due to the well known cooperative UC process of Yb^{3+} pairs in these host lattices.[50] The Yb^{3+} NIR and Yb^{3+} pair luminescence decay times found at 12 K in the $CsCdBr_3:3.8\%Ni^{2+},0.3\%Yb^{3+}$ ($\tau_{Yb^{3+}}=600$ μs and $\tau_{Yb^{3+}pairs}=285$ μs, respectively) agree well with the ratio 2/1 expected theoretically. An analogous result is obtained for the $CsMgBr_3:4.9\%Ni^{2+},0.6\%Yb^{3+}$, where the measured decay times are $\tau_{Yb^{3+}}=300$ μs and $\tau_{Yb^{3+}pairs}=170$ μs.

It is important to note that two subsets of Yb^{3+} ions are present in these codoped compounds, i.e., Yb^{3+} with and without a Ni^{2+} as a next neighbor. In both compounds around 10% of the Yb^{3+} ions have a Ni^{2+} nearest neighbor. Figures 3(b) and 4(b) show that after direct Ni^{2+} excitation at 20 491 cm^{-1} (12 K) not only Ni^{2+} but also Yb^{3+} luminescence is observed, and this is experimental evidence for a Ni^{2+} $^1T_{2g} \rightarrow Yb^{3+}$ $^2F_{5/2}$ energy transfer. We have measured the Yb^{3+} decay time after Ni^{2+} $^3T_{1g}(^3P)$ excitation at 20 491 cm^{-1} (see Tables I and II). It is reasonable to assume that in this experiment mainly Yb^{3+} ions with Ni^{2+} as a nearest neighbor are probed. The dominant decay component of this Yb^{3+} subset is 500 and 330 μs for $CsCdBr_3:3.8\%Ni^{2+},0.3\%Yb^{3+}$ and $CsMgBr_3:4.9\%Ni^{2+},0.6\%Yb^{3+}$, respectively at 12 K. The decay characteristics of this latter Yb^{3+} subset will be relevant for the discussion of the Ni^{2+} upconversion in Sec. IV D.

C. Ni^{2+} spectroscopy

Under 20 491 cm^{-1} excitation into the $^3T_{1g}(^3P)$ state, 12 K Ni^{2+} luminescence spectra of the title compounds show IR

broad emission bands centered around 5000 cm^{-1} and ascribed to the $^3T_{2g} \rightarrow {}^3A_{2g}$ transition. $CsCdBr_3:Ni^{2+},Yb^{3+}$ furthermore exhibits a broad luminescence band in the VIS region assigned to the Ni^{2+} $^1T_{2g} \rightarrow {}^3A_{2g}$ transition. $CsMgBr_3:Ni^{2+},Yb^{3+}$ shows an additional sharp luminescence feature at 16 760 cm^{-1} ascribed to the $^1A_{1g} \rightarrow {}^3A_{2g}$ spin-flip transition [see Fig. 4(b)]. In this host lattice the origins of the $^1T_{2g}$ and the $^1A_{1g}$ band are close in energy and, even at 12 K, luminescence from both states is observed. The different spectra obtained in the two compounds can be rationalized by crystal field theory. In Ni^{2+} only doped compounds, the magnitude of the crystal field strength, 10 Dq (mainly governed by the size of the M^{2+} ion of the host lattice), and the covalency, parameter B, determine whether the higher lying emitting state is the $^1T_{2g}$ or the $^1A_{1g}$. In $CsCdBr_3:Ni^{2+}$, red luminescence is observed from the $^1T_{2g}$ state, and $MgBr_2:Ni^{2+}$ shows $^1A_{1g}$ luminescence. $CsMgBr_3:Ni^{2+}$ represents an intermediate situation, and dual luminescence from both states is observed.[44]

After Yb^{3+} excitation in $CsCdBr_3:Ni^{2+},Yb^{3+}$ and $CsMgBr_3:Ni^{2+},Yb^{3+}$ the Ni^{2+} $^1T_{2g} \rightarrow {}^3A_{2g}$ luminescence is redshifted by 450 and 970 cm^{-1}, respectively, compared to direct green excitation into Ni^{2+} (see Figs. 3 and 4). We conclude that the emissions induced by green and NIR excitation originate from different subsets of Ni^{2+} ions in the crystal. Excitation into the $^3T_{1g}(^3P)$ broad absorption band at 20 491 cm^{-1} leads to the promotion of all Ni^{2+} ions to the upper emitting state in the crystal, regardless of their crystal field surrounding. But by Yb^{3+} excitation only Ni^{2+} ions close to Yb^{3+} are excited in an upconversion process to the $^1T_{2g}$ emitting state. The stronger axial crystal field induced by the presence of Yb^{3+} as the nearest neighbor is the origin of the observed redshifts. The larger mismatch of the ionic radii between the Mg^{2+} and Yb^{3+} in $CsMgBr_3$ ($R_{Mg^{2+}}$ =0.72 Å, $R_{Cd^{2+}}$=0.95 Å, $R_{Ni^{2+}}$=0.69 Å, and $R_{Yb^{3+}}$=0.87 Å) explains its stronger redshift compared to $CsCdBr_3$. In Fig. 4(b), a shoulder is observed in the low-energy region of the $^1T_{2g} \rightarrow {}^3A_{2g}$ emission band, at around 14 600 cm^{-1}. The shoulder lies at the same energy as the Ni^{2+} $^1T_{2g} \rightarrow {}^3A_{2g}$ emission after Yb^{3+} excitation. This is direct evidence that both Ni^{2+} subsets are excited at 20 491 cm^{-1}.

In both $CsCdBr_3:Ni^{2+},Yb^{3+}$ and $CsMgBr_3:Ni^{2+},Yb^{3+}$, Ni^{2+} $^1T_{2g} \rightarrow {}^3T_{2g}$ interexcited state luminescence is absent in the UC emission spectra after Yb^{3+} excitation. However, it is present after direct Ni^{2+} excitation. This interexcited state transition is overlapping with the Yb^{3+} $^2F_{7/2} \rightarrow {}^2F_{5/2}$ absorption, and thus we attribute its absence to the energy transfer from Ni^{2+} to Yb^{3+} near neighbor ions discussed in Sec. IV B. The absence of this interexcited state luminescence after Yb^{3+} excitation and the strong Yb^{3+} luminescence which is observed instead, proves that this energy transfer is efficient. This is an important result because the reverse process, i.e., the $Yb^{3+} \rightarrow Ni^{2+}$ energy transfer process, will be relevant for the upconversion.

D. Upconversion mechanism

There are broad features in the UC excitation spectra of Figs. 5(a) and 6(a) above 11 200 cm^{-1} for $CsCdBr_3:Ni^{2+},Yb^{3+}$ and 11 355 cm^{-1} for $CsMgBr_3:Ni^{2+},Yb^{3+}$, respectively. This band is also observed in the only Ni^{2+}-doped title compounds[44] and is assigned to a GSA/ESA UC process on the Ni^{2+} dopant ion. The sequence $^3A_{2g} \rightarrow {}^3T_{1g}, {}^1E_g$ (GSA) and $^3T_{2g} \rightarrow {}^1T_{2g}$ (ESA), involves rapid multiphonon relaxation from $^3T_{1g}$, ^1E_g to $^3T_{2g}$ after the GSA step.

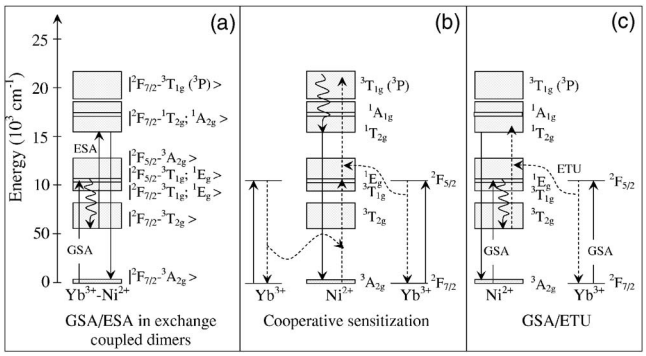

FIG. 10. Schematic illustration of three potential upconversion mechanisms in Ni^{2+},Yb^{3+} codoped $CsCdBr_3$ and $CsMgBr_3$. Solid arrows represent radiative processes, curly arrows multiphonon relaxation processes and dashed arrows nonradiative energy transfer processes.

Figure 10(a) shows a potential sequence of radiative GSA and ESA steps within a Ni^{2+}-Yb^{3+} pair model. This process is analogous to the GSA/ESA mechanism found in a variety of Mn^{2+} hosts doped with Yb^{3+} (Refs. 14, 16, 18–20, 23, and 24) or codoped Mn^{2+} and Yb^{3+} lattices.[22] However, there are two important differences between our compound and the Mn^{2+}-Yb^{3+} systems. In most of the latter, every Yb^{3+} is close to a Mn^{2+} ion and, more importantly, in our system the Yb^{3+} $^2F_{5/2}$ excited state is resonant with Ni^{2+} $^3T_{1g}$ state. Figure 10(b) depicts a possible UC mechanism based on cooperative sensitization of one Ni^{2+} ion by two Yb^{3+} excitations. Such a cooperative sensitization UC mechanism involving three ions has been already proposed for Cr^{3+}-Yb^{3+}(Refs. 25–27) and Tb^{3+}-Yb^{3+}[57–59] systems. This would be favored by the spectral overlap of the Yb^{3+} emission with the $^3T_{1g}(^3P)$ Ni^{2+} absorption band.

Figure 10(c) presents the last potential mechanism, i.e., the GSA/ETU process in an Yb^{3+}-Ni^{2+} pair. In a first step Ni^{2+} is excited to the $^3T_{2g}$ state either by direct absorption of a laser photon or by energy transfer from a neighboring Yb^{3+} ion. The second step corresponds to an energy transfer from Yb^{3+} $^2F_{5/2} \rightarrow {}^2F_{7/2}$ to Ni^{2+} $^3T_{2g} \rightarrow {}^1T_{2g}$.

Fingerprint of the UC mechanism are found in the decay curves of the UC luminescence shown in Fig. 9. The intrinsic lifetime of Ni^{2+} $^1T_{2g}$ state, i.e., after direct Ni^{2+} excitation, is 2.7 μs and 6.8 μs for $CsCdBr_3$: 3.8% Ni^{2+}, 0.3% Yb^{3+} [Fig. 9(b)] and $CsMgBr_3$: 4.9% Ni^{2+}, 0.6% Yb^{3+}, respectively (see Tables I and II). These values are in good agreement with the lifetimes of this state in the corresponding Ni^{2+}

single doped compounds.[39,44] For the scenario shown in Fig. 10(a), one would predict a lifetime of the UC emission around 2.7 and 6.8 μs for the Cd^{2+} and Mg^{2+} host lattice, respectively, or even smaller due to the additional deactivation channels, such as the energy transfer from Ni^{2+} to Yb^{3+}. However, the measured Ni^{2+} $^1T_{2g}$ UC decay time after Yb^{3+} excitation in $CsCdBr_3:3.8\%\,Ni^{2+},0.3\%\,Yb^{3+}$ is 420 μs [Table I, Fig. 9(a)] and $\tau=330$ μs for the $CsMgBr_3:4.9\%\,Ni^{2+},0.6\%\,Yb^{3+}$ (Table II). Consequently, we can rule out the GSA/ESA mechanism in Fig. 10(a).

If a cooperative sensitization mechanism as depicted in Fig. 10(b) were to induce the UC luminescence, the Ni^{2+} $^1T_{2g}$ lifetime should be at most half that of the Yb^{3+}. This is because two excited Yb^{3+} ions cooperatively transfer their energy to a Ni^{2+} ion. This situation is closely related to the Yb^{3+} pair luminescence discussed above. The decay time of the Yb^{3+} pair are $\tau=285$ and 170 μs for $CsCdBr_3:3.8\%\,Ni^{2+},0.3\%\,Yb^{3+}$ and $CsMgBr_3:4.9\%\,Ni^{2+}$, $0.6\%\,Yb^{3+}$, respectively. The observed Ni^{2+} $^1T_{2g}$ UC decay time of 420 and 330 μs are significantly larger and we discard the cooperative sensitization mechanism in Fig. 10(b). Additional evidence to rule out such a mechanism is finally found in the power dependence data presented in Fig. 8. There one sees that the slope of the Yb^{3+} pair luminescence is 2 over the whole power range. If the Ni^{2+} UC luminescence was based on the cooperative energy transfer from Yb^{3+} pairs, the power dependence of the Ni^{2+} luminescence should not reduce from 2.1 ± 0.1 to 1.3 ± 0.1 but always follow the power dependence of the Yb^{3+} pairs.

For the mechanism in Fig. 10(c) the UC Ni^{2+} $^1T_{2g}$ decay is expected to be governed by the lifetime of the energy storage reservoirs involved. The Ni^{2+} $^3T_{2g}$ state is one of these and has a lifetime $\tau=8.1$ ms in the Cd^{2+} lattice. The second energy storage reservoir is the $^2F_{5/2}$ state of Yb^{3+} ions next to a Ni^{2+}. The decay time of this Yb^{3+} subset is $\tau=500$ μs in the Cd^{2+} lattice. The sum of the decay rate constants of the two reservoirs should equal the measured rate constant of the Ni^{2+} upconversion. We thus estimate a Ni^{2+} $^1T_{2g}$ lifetime of 471 μs for the $CsCdBr_3:3.8\%\,Ni^{2+},0.3\%\,Yb^{3+}$. This value agrees well with the measured decay time of 420 μs for the Ni^{2+} $^1T_{2g}$ UC emission after 10 604 cm^{-1} excitation. In the Mg^{2+} host lattice the decay time of the relevant Yb^{3+} subset and the Ni^{2+} UC are both around 330 μs. This is strong evidence for the mechanism in Fig. 10(c) for both host lattices.

This is supported by a recent theoretical model for the power dependence of UC luminescence based on a GSA/ETU mechanism, where the sensitizer and the emitting ion are not the same species.[60] This model predicts that the slope of the UC luminescence reduces from 2 to 1 in the high power limit, in agreement with the power dependence data of $CsCdBr_3:Ni^{2+},Yb^{3+}$ presented in Fig. 8(b). Sample heating in the high power regime can be ruled out due to the fact that the power dependence of the Yb^{3+} pair luminescence is 2 over the whole measured power range.

From the absorption spectra shown in Fig. 1, we deduce that an excitation energy provided by the Yb^{3+} is not sufficient to reach the upper emitting level $^1T_{2g}$ from the $^3T_{2g}$ Ni^{2+} state. At first sight, this is in contradiction to the process in Fig. 10(c). But one has to bear in mind that the absorption spectrum probes the vast majority of the "isolated" Ni^{2+} ions. The $^3T_{2g}\rightarrow{}^1T_{2g}$ energy gap for Ni^{2+} ions with an Yb^{3+} nearest neighbor (described in Sec. IV C) is at least 450 and 970 cm^{-1} lower than for the "isolated" Ni^{2+} ions in the Cd and Mg host lattices, respectively. By this reduction the ETU step becomes energetically accessible for nearest neighbor Yb^{3+}-Ni^{2+} pairs.

E. Upconversion efficiency

The efficiency of the UC process can be estimated from the ratio of the VIS Ni^{2+} $^1T_{2g}$ UC photons to TOTAL photons emitted from the samples after excitation around 10 600 cm^{-1}. This ratio is temperature and power dependent because UC is a non linear process. According to the statistical distribution of the Ni^{2+} ions described in Sec. IV A, and taking into account that around 10 600 cm^{-1} we excite also "isolated" Ni^{2+} ions into the $^3T_{1g}/{}^1E_g$ states, the estimated fraction of red Ni^{2+} UC to the total emitted photons is about 1% for both title compounds at 12 K and for an excitation power density around 4.7 kW/cm^2. This is a surprisingly high number if one takes into account that the $^1T_{2g}$ to $^3T_{2g}$ photon ratio after direct Ni^{2+} excitation into the $^3T_{1g}(^3P)$ state is around 2.5% for the singly doped bromide systems.[44] The ETU step in Fig. 10(c) apparently is efficient, but so is the reverse process, which acts as the major loss mechanism for the UC luminescence and according to Fig. 7 is thermally activated.

Thus, resonant laser excitation into the Yb^{3+} $^2F_{5/2}$ absorption around 10 600 cm^{-1} induces more efficient Ni^{2+} $^1T_{2g}$ UC luminescence than the single-ion GSA/ESA process within the Ni^{2+} ions observed for excitation energies above 11 200 cm^{-1}.

Based on previous studies, the VIS to total photon ratios in Mn-Yb systems are strongly dependent on the host lattice. We were tempted to carry out an analogous analysis on different doubly doped $Ni^{2+}-Yb^{3+}$ halides lattices. Nevertheless, neither $Rb_2CdCl_4:Ni^{2+},Yb^{3+}$ nor $CsCdCl_3:Ni^{2+},Yb^{3+}$ exhibit Ni^{2+} VIS luminescence after Yb^{3+} excitation. The ETU step is certainly strongly dependent on the distance of the active ion and in the case of the $Rb_2CdCl_4:Ni^{2+},Yb^{3+}$ the dopant sites have a significantly larger separation than in the title compounds and this might explain the absence of the UC luminescence. However, in the case of $CsCdCl_3:Ni^{2+},Yb^{3+}$ there are dopant sites available that have a similar separation and geometrical arrangement as in the title compounds. This suggests that the nature of the halide and the change in 10 Dq/B (crystal field to covalency ratio) are the key factors for the UC efficiency. At this point this is somewhat speculative and we are exploring other halides lattices to better understand these phenomena.

V. CONCLUSIONS

We have observed and characterized an upconversion phenomenon in a new trasition-metal–rare-eath system, Ni^{2+}/Yb^{3+}. Upon Yb^{3+} $^2F_{5/2}$ excitation, the $CsMBr_3:Ni^{2+},Yb^{3+}$ ($M=Cd^{2+},Mg^{2+}$) exhibit red Ni^{2+} $^1T_{2g}$ UC luminescence at low temperatures.

Lifetime measurements in combination with power dependence data allow a distinction between potential UC mechanisms. The Ni^{2+} $^1T_{2g}$ upconversion is assigned to a GSA/ETU mechanism. The Ni^{2+} distortion caused by the presence of neighboring Yb^{3+} shifts the Ni^{2+} energy levels to facilitate the ETU step energetically.

This UC process via Yb^{3+} excitation is more efficient than the GSA/ESA upconversion process in Ni^{2+} single ions. The UC efficiency for excitation via Yb^{3+} is limited by the back transfer from the Ni^{2+} $^1T_{2g}$ state to Yb^{3+} $^2F_{5/2}$ level which is the reverse process of the ETU step. The luminescence quenches at temperatures around 100 K due to multiphonon relaxation processes. This effect is also observed in many other singly doped Ni^{2+} systems. However, it sets in at slightly lower temperatures for Ni^{2+} UC luminescence after Yb^{3+} NIR excitation. The results of the present study are encouraging to investigate the UC properties of the Ni^{2+}/Yb^{3+} couple in other lattices in order to shed more light on the role played by different geometrical parameters and ligands.

ACKNOWLEDGEMENTS

The authors are grateful to M. Pollnau, J. M. García-Lastra, and F. Rodríguez for fruitful discussions. This work was financially supported by the Spanish Ministerio de Ciencia y Tecnología (MCyT) under Project No. BFM-2001-0695 and by the Swiss National Science Foundation.

[1] J. C. Wright, *Topics in Applied Physics: Radiationless Processes in Molecules and Condensed Phases* (Springer, Berlin, 1976).
[2] M. F. Joubert, Opt. Mater. **11**, 181 (1999).
[3] E. Downing, L. Hesselink, J. Ralston, and R. M. Macfarlane, Science **273**, 1185 (1996).
[4] M. P. Hehlen, M. L. F. Phillips, N. J. Cockroft, and H. U. Güdel, *Upconversion Phosphors* (Pergamon, Oxford, 2001).
[5] J. S. Chivian, W. E. Case, and D. D. Eden, Appl. Phys. Lett. **35**, 124 (1979).
[6] D. R. Gamelin and H. U. Güdel, Top. Curr. Chem. **214**, 1 (2001).
[7] F. Auzel, Chem. Rev. (Washington, D.C.) **104**, 139 (2004).
[8] S. M. Jacobsen and H. U. Güdel, J. Lumin. **43**, 125 (1989).
[9] U. Oetliker, M. J. Riley, P. S. May, and H. U. Güdel, J. Lumin. **53**, 553 (1992).
[10] D. R. Gamelin and H. U. Güdel, J. Am. Chem. Soc. **120**, 12143 (1998).
[11] D. R. Gamelin, M. Wermuth, and H. U. Güdel, J. Lumin. **83-4**, 405 (1999).
[12] M. Wermuth and H. U. Güdel, J. Am. Chem. Soc. **121**, 10102 (1999).
[13] F. Varsanyi and G. H. Dieke, Phys. Rev. Lett. **7**, 442 (1961).
[14] R. Valiente, O. S. Wenger, and H. U. Güdel, Chem. Phys. Lett. **320**, 639 (2000).
[15] O. S. Wenger, D. R. Gamelin, and H. U. Güdel, J. Am. Chem. Soc. **122**, 7408 (2000).
[16] P. Gerner, O. S. Wenger, R. Valiente, and H. U. Güdel, Inorg. Chem. **40**, 4534 (2001).
[17] O. S. Wenger, R. Valiente, and H. U. Güdel, Phys. Rev. B **64**, 235116 (2001).
[18] C. Reinhard, P. Gerner, R. Valiente, O. S. Wenger, and H. U. Güdel, J. Lumin. **94-95**, 331 (2001).
[19] R. Valiente, O. Wenger, and H. U. Güdel, Phys. Rev. B **63**, 165102 (2001).
[20] C. Reinhard, R. Valiente, and H. U. Güdel, J. Phys. Chem. B **106**, 10 051 (2002).
[21] R. Valiente, O. S. Wenger, and H. U. Güdel, J. Chem. Phys. **116**, 5196 (2002).
[22] C. Reinhard, P. Gerner, F. Rodríguez, S. García-Revilla, R. Valiente, and H. U. Güdel, Chem. Phys. Lett. **386**, 132 (2004).
[23] P. Gerner, C. Reinhard, and H. U. Güdel, Chem.-Eur. J. **10**, 4735 (2004).
[24] P. Gerner, C. Fuhrer, C. Reinhard, and H. U. Güdel, J. Alloys Compd. **380**, 39 (2004).
[25] S. Heer, M. Wermuth, K. Krämer, D. Ehrentraut, and H. U. Güdel, J. Lumin. **94-95**, 337 (2001).
[26] S. Heer, M. Wermuth, K. Krämer, and H. U. Güdel, Chem. Phys. Lett. **334**, 293 (2001).
[27] S. Heer, M. Wermuth, K. Krämer, and H. U. Güdel, Phys. Rev. B **65**, 125112 (2002).
[28] A. Aebischer and H. U. Güdel, J. Alloys Compd. **374**, 60 (2004).
[29] C. Reinhard, K. Krämer, D. A. Biner, and H. U. Güdel, J. Chem. Phys. **120**, 3374 (2004).
[30] M. Kasha, Discuss. Faraday Soc. **9**, 14 (1950).
[31] L. F. Johnson, R. E. Dietz, and H. J. Guggenheim, Phys. Rev. Lett. **11**, 318 (1963).
[32] P. F. Moulton, *Tunable Paramagnetic-ion Lasers* (North-Holland, Amsterdam, 1985).
[33] L. F. Johnson, H. J. Guggenheim, D. Bahnck, and A. M. Johnson, Opt. Lett. **8**, 371 (1983).
[34] R. Moncorgé and T. Benyattou, Phys. Rev. B **37**, 9186 (1988).
[35] P. S. May and H. U. Güdel, Chem. Phys. Lett. **164**, 612 (1989).
[36] P. S. May and H. U. Güdel, J. Lumin. **46**, 277 (1990).
[37] U. Oetliker, M. J. Riley, P. S. May, and H. U. Güdel, Coord. Chem. Rev. **111**, 125 (1991).
[38] P. S. May and H. U. Güdel, J. Chem. Phys. **95**, 6343 (1991).
[39] D. de Viry, N. Tercier, J. P. Denis, B. Blanzat, and F. Pellé, J. Chem. Phys. **97**, 2263 (1992).
[40] F. Lahoz, M. Díaz, B. Villacampa, R. Cases, and R. Alcalá, J. Appl. Phys. **82**, 5121 (1997).
[41] J. Grimm, O. S. Wenger, and H. U. Güdel, J. Lumin. **102-103**, 380 (2003).
[42] O. S. Wenger and H. U. Güdel, Inorg. Chem. **40**, 157 (2001).
[43] O. S. Wenger, G. M. Salley, R. Valiente, and H. U. Güdel, Phys. Rev. B **65**, 212108 (2002).
[44] O. S. Wenger, S. Bénard, and H. U. Güdel, Inorg. Chem. **41**, 5968 (2002).
[45] O. S. Wenger and H. U. Güdel, Struct. Bonding (Berlin) **106**, 59 (2004).
[46] O. S. Wenger, R. Valiente, and H. U. Güdel, High Press. Res. **22**, 57 (2002).
[47] S. García-Revilla, P. Gerner, O. S. Wenger, H. U. Güdel, and R. Valiente, Chem. Phys. Lett. **401**, 492 (2005).

[48] G. L. McPherson, A. M. McPherson, and J. L. Atwood, J. Phys. Chem. Solids **41**, 495 (1980).
[49] S. Sugano, Y. Tanabe, and H. Kamimura, *Multiplets of Transition Metal Ions in Crystals* (Academic Press, New York, 1970).
[50] Ph. Goldner, F. Pellè, D. Meichenin, and F. Auzel, J. Lumin. **71**, 137 (1997).
[51] B. Z. Malkin, A. M. Leushin, A. I. Iskhakova, J. Heber, M. Altwein, K. Moller, I. I. Fazlizhanov, and V. A. Ulanov, Phys. Rev. B **62**, 7063 (2000).
[52] V. Mehta and D. Gourier, J. Comput. Phys. **13**, 4567 (2001).
[53] V. Mehta, O. Guillot-Noel, D. Simons, D. Gourier, P. Goldner, and F. Pellé, J. Alloys Compd. **323-324**, 308 (2001).
[54] L. M. Henling and G. L. McPherson, Phys. Rev. B **16**, 4756 (1977).
[55] M. P. Hehlen, A. Kuditcher, S. C. Rand, and M. A. Tischler, J. Chem. Phys. **107**, 4886 (1997).
[56] G. L. McPherson and L. M. Henling, Phys. Rev. B **16**, 1889 (1977).
[57] G. M. Salley, R. Valiente, and H. U. Güdel, J. Lumin. **94-95**, 305 (2001).
[58] G. M. Salley, R. Valiente, and H. U. Güdel, J. Phys.: Condens. Matter **14**, 5461 (2002).
[59] G. M. Salley, R. Valiente, and H. U. Güdel, Phys. Rev. B **67**, 134111 (2003).
[60] J. F. Suyver, A. Aebischer, S. García-Revilla, P. Gerner, and H. U. Güdel, Phys. Rev. B **71**, 125123 (2005).